



Method to Detect Arc Across Pantograph-Catenary Structure Atop Train Based on Frequency Features of Entry Current

Yufei Du^{1,2}(✉) , Yang Jiao² , Yongzheng Zhu² , Jun Chen² , Hongbin Li² , and Qing Chen³

¹ Institute of Artificial Intelligence, Huazhong University of Science and Technology, Wuhan 430074, China

530891333@qq.com, trinitysphinx@gmail.com

² School of Electrical and Electronics Engineering, Huazhong University of Science and Technology, Wuhan 430074, China

³ State Key Laboratory of Advanced Electromagnetic Engineering and Technology, Huazhong University of Science and Technology, Wuhan 430074, China

Abstract. During a train running at speed, the pantograph-catenary structure atop the train would be influenced by many factors, resulting in disconnections. A timely detection on arcs across this structure helps to guide works on real-time operating and later maintenance, to eliminate latent factors of disconnection. A theory on the generation of arcs is researched, simulated, and verified with practical data. Two features of entry current, in frequency bands at kHz degree and at harmonic-Hz degree, are picked for the detection. Based on the discrepancy on these bands while arcing and normally running, a model of support vector machine (SVM) is constructed. Existing signals on train are processed and rearranged to be datasets for training SVM. After applying it to a practical railway, the results illustrate: the accuracy on arc detections is up to 99.96%. With guidance from results, an on-site investigation was launched, and mark of flaming was found at corresponding location of catenary, which verified the correctness.

Keywords: Electrical locomotive · Arc detection · Frequency feature · SVM

1 Introduction

Electrical locomotives get power based on the sliding contact of the pantograph over train and the catenary of power network [1–3]. Many factors would harm this contact, such as uneven ground surface, deformations on pantograph, and others. As a result, the gap between pantograph-catenary structure (P-C structure) would be broken down by high voltage, and an arc between P-C structure (PCArc) is generated. It leaves potential issues to railway system such as P-C structure flamed to further deformation. Therefore, A timely detection on arc across this structure helps to guide works on real-time operating and later maintenance.

Existing researches on PCArc, mainly focus on 3 aspects: The **first** type employs specific equipment to capture physical features of PCArc such as sound, light, and electromagnetic waves [4–6]. In paper [4], light spectra of PCArc were analyzed. The wavelength around 250 ± 10 nm was proposed as the criterion to detect PCArc. In addition, an optical detection system, including an ultraviolet sensor and data analyzing device, was designed to implement the method. In paper [5], sounds of arc are analyzed, and the frequency band (5–17 kHz) of arc, was extracted with noise reduced and filtered. This band was then used as a criterion for determining parameters such as the arc-occurring time and the off-line rate. Although applications of specific equipment have been proved effective, it results in more cost on maintenance for train. Additionally compared with electrical signal measurement, employing specific equipment is more likely to be interfered due to complex environment of railway. Therefore, it's not widely used. For the **second** type, self-build P-C structures [7, 8] were applied and simulated in isolated lab environments. Commonly, a setup with dual-rod structure was used to simulate the connection of P-C structure. At the end of the circuit model, an equivalent inductive load was here to simulate the transformer on train. In paper [9], a platform was constructed to research arc feature, including arc peak voltage at steady-state offline or dynamic offline. By observing the asymmetry in volt-ampere curve during arcing, PCArc could be detected effectively. In paper [10], entry currents of locomotive under various conditions were researched and analyzed to classify the state of arcing or normal. Then, an online method to detect PCArc based on SVM was proposed. However, replicating a P-C structure in lab to simulate the practical is challenging. The difference between the artificial arc and PCArc relies on the comprehension of experimenters on arc largely. Thus, further researches are necessary to verify its correctness. The **third** type detects PCArc by using the features from electrical signal on train. For example, classical Cassie-Mayr black-box models were applied in papers [11, 12], then empirical formulas were applied to simulate the time-various conductors of PCArc. In paper [13], PCArc was modeled as a series of 2 conductors, corresponding to a high-current region and a low-current region. With massive experimental data, relationships from dissipated power to train speed, and to length of gap were established, to optimize this model. Similar models effectively replicated the phenomenon of zero-Amp period while arc current was crossing zero-Amp axis, thus they were widely applied in fields like gas isolated switchgear (GIS) [14, 15]. However, power of frequency features (FqF) of a zero-Amp period is focused on a band of several-hundred-Hz, which is interfered easily by harmonic from the power grid, thus, further studies on PCArc, especially on more FqFs and the generation theory of arcs, are essential for optimization.

Considering all above, a method to detect arc across based on FqFs of entry current is proposed in this paper: Firstly, theory on generation of PCArc is researched, simulated, and verified with practical data. Two features of entry current, in frequency bands at kHz degree and at harmonic-Hz degree, are picked for detection. Then, SVM is constructed based on the discrepancy on these bands. With the labels supplied from “Running state of train and power grid monitor” (3C device), entry current is processed and rearranged as datasets, and the hyperplane of SVM is solved. After applying it to a practical railway, the accuracy of the proposed method can be calculated quantitatively. Finally, an on-site

investigation was launched, and mark of flaming was found at corresponding location of catenary, which verified the correction of the proposed method.

2 Frequency Features of Entry Current

2.1 Theory and Researches on PCArc

The voltage level of electrical railway system in China is 25 kV at 50 Hz. The power is transported through the P-C structure and a coaxial cable to the transformer on train. For the sake of simplicity, current flow through this circuit is named as entry current (i_E). When the gap between P-C structure is broken down by 25-kV voltage, all units in this circuit are in series, which is displayed in Fig. 1.

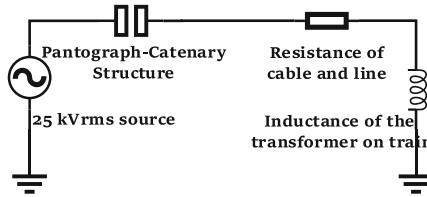


Fig. 1. Equivalent circuit while arcing

The whole power-supply network is influenced very weakly while arcing, thus it can be regarded as a voltage source with no fluctuation:

$$E_s(t) = 25\sqrt{2} \sin(100\pi \cdot t) \quad (1)$$

According to existing studies [14, 15] on arcs: With the gap between P-C structure broken down, it is equivalent to a time-varying conductor $g_A(t)$, i.e. Equation (2). The full life cycle of an arc can be divided into 3 stages. A variable Q is used to describe: arc starting ($Q = 1$, stage 1), arcing steadily ($Q = 2$, stage 2) and arc fading ($Q = 3$, stage 3).

$$g_A(t) = \begin{cases} \frac{1}{R_0(\frac{t_\delta}{t-t_0} - 1) + R_s}, & Q = 1 \\ \frac{1}{R_s}, & Q = 2 \\ g_A(t-dt) + \frac{dt}{\tau_M} \left\{ E_s(t-dt) - i_A(t-dt) \left[R_0 + \frac{1}{g_A(t-dt)} \right] \right\}, & Q = 3 \end{cases} \quad (2)$$

where $i_A = i_E$ denotes the current flowing through the arc. $R_0 = 10^{12}\Omega$ denotes the equivalent resistance before gap is broken down. Mark t_0 as the moment corresponding to breakdown. The time span of stage 1 is t_δ , which is related to the type of air in the

gap. $R_s = 4\Omega$ is the equivalent resistance of PCArc during stage 2. $\tau_M = 1.5 \times 10^{-6}$ is a constant in this model.

Stage 3 begins when i_A crossing zero-Amp axis, i.e. Equation (3) is not satisfied any more.

$$\begin{cases} K > |i_A(t) - i_A(t - Ldt)| \\ i_A(t) \cdot i_A(t - Ldt) < 0 \end{cases} \quad (3)$$

where L and K are used to control the length of time and the extent of current-drop. During stage 3, if the voltage u_A across the gap growing to a degree over breakdown voltage u_{Ex} , i.e. Equation (4) is satisfied, stage 3 would be changed to stage 1.

$$|u_A(t)| = \left| \frac{i_A(t)}{g_A(t)} \right| > u_{Ex}(t) \quad (4)$$

During the whole life cycle of arcing, three stages mentioned above changes to each other, until the P-C structure is closed or disconnected totally.

Based on the model in Fig. 1, Eq. (5) can be derived with Kirchoff's voltage law:

$$L \frac{di_A(t)}{dt} + Z_0 i_A(t) + \frac{i_A(t)}{g_A(t)} = E_s(t) \quad (5)$$

After discretizing, it is converted to:

$$i_A(t) = \frac{dt}{L} \left\{ E_s(t - dt) - \left[Z_0 + \frac{1}{g_A(t - dt)} \right] \cdot i_A(t - dt) \right\} \quad (6)$$

while i_A getting across zero-Amp (name this time span as zero-Amp period), the initial value of $i_A(t - dt)$ is near zero, thus for most time during this span:

$$i_A(t)|_{i_A(t-dt) \rightarrow 0} \approx \frac{dt}{L} E_s(t - dt) \ll 1 \quad (7)$$

It shall be mentioned that after the gap is broken down, some time is needed for the air in gap, to ensure u_{Ex} recovering to its quiescent value. During this time, u_A is still large enough to break down the gap once more, i.e. stage 3 is transformed to stage 1. However, i_A is very weak during zero-Amp period, that makes the time span of stage 2 is very short. Therefore, stage 1 and stage 3 are changed to each other quickly. This phenomenon results in the value of $\frac{i_A(t-dt)}{g_A(t-dt)}$ rising and dropping frequently.

Considering all above, two visible components in frequency domain can be observed: On the one hand, zero-Amp period makes the waveform of i_A not smooth, thus many components at harmonic-Hz (HNC) can be obtained in frequency domain after FFT. On the other hand, frequent changing between stage 1 and stage 3 results to components with k-Hertz frequency (kHC).

2.2 Simulations on PCArc

Features of HNC and kHC can be verified with simulation. Suppose: the equivalent inductance of transformer on train is $L \approx 5$ mH. The resistance of cable is $Z_0 \approx 30\Omega$. u_{Ex} is related to the distance of air gap:

$$u_{Ex}(t) = E_0(D_0 - vt) \quad (8)$$

where: $E_0 \approx 30$ kV/cm is the breakdown voltage across per-unit gap length. $D_0 = 1.29$ m is the distance between pantograph and catenary. Pantograph rises with speed $v = 0.5$ m/s. For a 25kV network, it's suggested to configure $K = 300$ and $L = 10$ in Eq. (3). For the solver of differential equation: The minimum of time dt is set to be 1 ns, with initial voltage $u_{A,0} = 0$ V and initial current $i_{A,0} = 0$ A. With all above, the voltage u_A across PCArc and the current i_A can be simulated as Fig. 2.

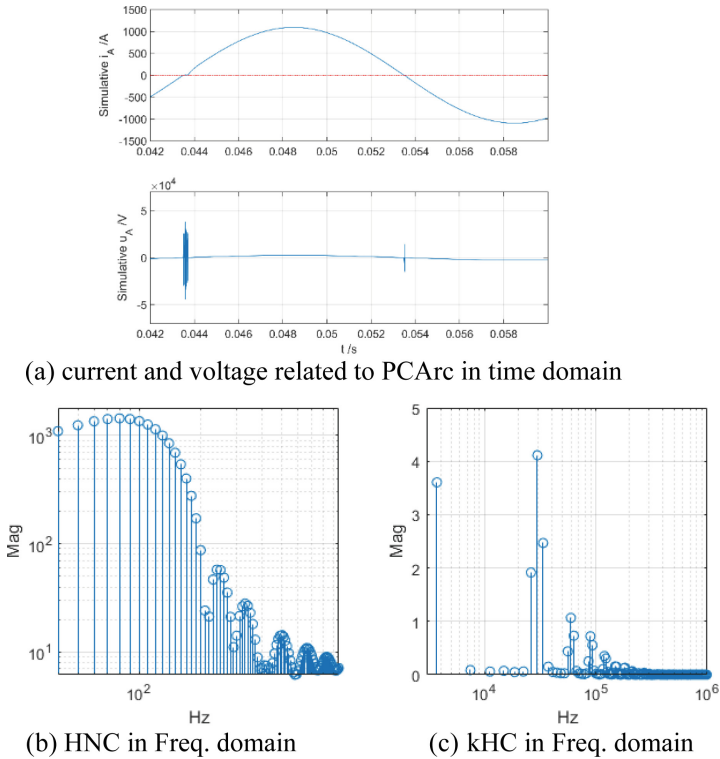


Fig. 2. Features of PCArc in frequency and time domain

Entry current $i_E = i_A$ through PCArc is shown in subfigure (a), and the zero-Amp period can be observed near the red line. Considering the kHC is not easy to be observed in current waveform, the phenomenon with frequent changing between stage 1 and stage 3 is displayed via u_A . In freq. Domain, the peaks of HNC locate at 250 Hz (57.1938 A) and 330 Hz (28.154 A), which is shown in subfigure (b). The signal fragment covering zero-Amp period is picked out and processed using FFT, which is shown in subfigure (c). Several remarkable peaks locate at 3.717 kHz (3.6047 A), 29.739 kHz (4.1122 A) and 59.479 kHz (1.0659 A).

2.3 Confirmation by Practical Waveforms

The features mentioned above can be confirmed by practical waveforms as well. Currents from a HXD1C-type train in 2021 are shown as examples: i_E is sensed via a Rogowski coil (Rog. Coil), then it's sampled by a high-speed data acquisition card (DAQ card). After de-gain the signal with the frequency-response curve of Rog. Coil, the spectra in freq. Domain can be displayed in Fig. 3.

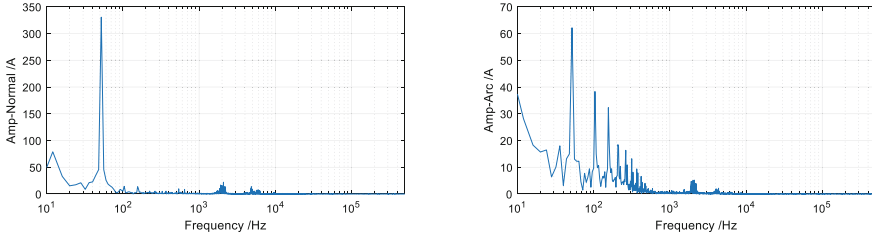


Fig. 3. Spectra of signals in normal and arcing

It can be illustrated from Fig. 3: During normal running, only the 3rd and the 5th harmonics are remarkable, and the kHC is very weak, whereas, during arcing, components less than 1 kHz and kHC rise sensibly. Although spectra are different from time to time, the huge diversity is large enough to serve as the basis to detect PCArc.

3 Principle to Detect PCArc

3.1 Scheme

The flowchart of detecting PCArc is shown in Fig. 4. After acquiring i_E , pre-processing, including windowed FFT, de-gaining and normalization, is necessary to convert huge time-domain analog signal to FqF with low dimension. In addition, a detection model is proposed to detect PCArc with proper criterions.

Two steps are significant in this scheme: (1) the approach of pre-processing shall be appropriate to ensure detecting PCArc precisely on the premise of compressing data. (2) An excellent detecting algorithm is critical as well. Considering these, a model of SVM is constructed to accomplish the detection of PCArc.

3.2 Key Steps

Data Pre-processing

To extract the frequency features of i_E , Hann-windowed FFT is applied to process the entry current. Suppose x denotes the discrete series sampled from i_E , with a length N , hence B_k the spectrum versus k in the freq. Domain is:

$$B_k \triangleq F_k\{x\} \approx \frac{A_z}{2j} e^{-j\varphi_z} \cdot W\left(k - f_z \frac{N}{F_s}\right) \quad (9)$$

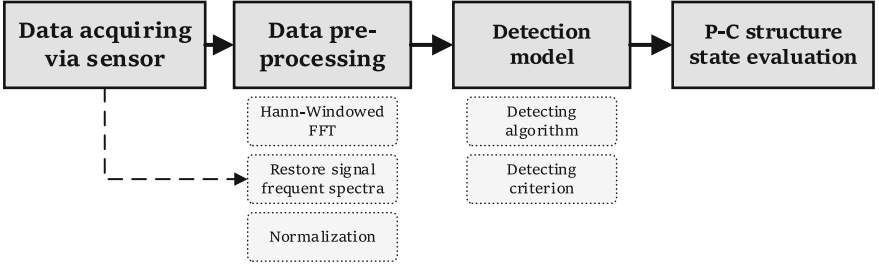


Fig. 4. Flowchart of the recognizing method

where F is the function of FFT. $W(\cdot)$ is the function of Hann window in freq. Domain. Variables A_z and φ_z are amplitude and phase respectively versus a sinusoid with frequency f_z . z is the index of sinusoids. When $k = f_z N / F_s$, the gain from Hann window to z -th sinusoid gets to the top, hence A_z could be derived according to B_k :

$$A_z = \left| \frac{2jB_k}{e^{-j\varphi_z} \cdot W(k' = 0)} \right| \rightarrow \left| \frac{2jB_k}{e^{-j\varphi_z} \cdot (N/2)} \right| = \frac{4|B_k|}{N} \quad (10)$$

After de-gaining the spectrum based on the frequency-response curve $G(f_z)$ of sensor, the real spectrum X_k of i_E at k -Hz can be obtained:

$$X_k = \frac{A_z}{G(f_z)} \quad (11)$$

According to the analysis in Sect. 2, features of PCArc appear in many aspects., thus, the effective freq. Band of the sensor can be divided with a multiple of 10, considering generality: Suppose m bands with index $j = 1, 2, \dots, m$ in freq. Domain are supposed to be generated. Feature corresponding to the m -th band can be calculated:

$$q_{i,j} = \frac{1}{H} \sum_{k \in \mathbf{F}_j} X_k^2, q_{i,j} = \frac{1}{H} \left[\sum_{k \in \{f_{st,j}, f_{ed,j}\}} X_k^2 + \frac{1}{2} X_{f_{st,j}}^2 + \frac{1}{2} X_{f_{ed,j}}^2 \right] \quad (12)$$

where H is the number of spectra in band $\mathbf{F}_j = [f_{st,j}, f_{ed,j}]$. If i_E is sampled and processed into p N -length signal fragments, with $i = 1, 2, \dots, p$, $q_{i,j}$ denotes the square-mean value in \mathbf{F}_j corresponding to the i -th fragment. Especially, for the spectrum at the boundary of \mathbf{F}_j , its power shall be shared to its 2 neighbor bands.

For each N -length fragment x , its $p \times m$ -dimension feature matrix $\mathbf{Q} = \{q_{i,j}\}$ can be computed, with Eqs. (9)–(12). Then a normalization to it in row is necessary. The reason is: Different components in freq. Bands possess different degrees of power, thus normalization helps to eliminate this interference.

$$\mathbf{Q}' = \{q'_{i,j}\}, q'_{i,j} = \frac{q_{i,j}}{\max_i q_{i,j}}, \mathbf{Q}'' = \{q''_{i,j}\}, q''_{i,j} = \frac{q'_{i,j}}{q'_{i,2}} \quad (13)$$

Then, a normalization in column is applied to the intermediate matrix $\mathbf{Q}' = \{q'_{i,j}\}$. Especially, the reference value for normalization is with $j = 2$. Reasons includes: (1)

band with $j = 2$ covers 50 Hz, which is the fundamental frequency, thus after normalizing, the meaning of this ratio contains better interpretability. (2) In railway's daily running, total-harmonic-distortion (THD) is commonly less than 1, thus it helps to analyze results quantitatively.

With all signal fragments processed via Eqs. (9)–(13), feature vectors \mathbf{Q}'' with several FqFs can be obtained, which is essential for solving hyperplane.

Detection

Solving a hyperplane by machine learning is the critical process of SVM. To realize this model, specimens \mathbf{S}_i shall be generated by rearranging elements in \mathbf{Q}'' in row:

$$\mathbf{S}_i = \{\mathbf{x}_i, y_i\}, \mathbf{x}_i = (q''_{i,j} | j = 1, 2, \dots, m) \quad (14)$$

where $y_i \in \{-1, +1\}$ denotes the output label of \mathbf{S}_i . According to the theory of SVM, if the features of \mathbf{S}_i match with PCArc, the corresponding label is marked to be +1, otherwise -1. In specimens' space, the hyperplane can be expressed:

$$y = \boldsymbol{\omega}^T \mathbf{x} + b \quad (15)$$

where $b \in \mathbf{R}$. $\boldsymbol{\omega} = (\omega_1, \omega_2, \dots, \omega_m) \in \mathbf{R}$ is the normal vector of hyperplane. The dimension of $\boldsymbol{\omega}$ equals to frequency features in the proposed method. Reflected in physic, if $\boldsymbol{\omega}$ is solved, the direction of the hyperplane can be known. If b is solved, the distance from hyperplane to origin can be known. An optimizing model is applied to solve them.

$$\min \frac{1}{2} \|\boldsymbol{\omega}\|^2, \quad \text{s.t. } y_i [\boldsymbol{\omega}^T \phi(\mathbf{x}) + b] \geq 1, i = 1, 2, \dots, p \quad (16)$$

where function $\phi(\mathbf{x})$ denotes mapping \mathbf{x} to a higher dimension. According to the deduction in pre-processing, the dimension of \mathbf{Q}'' is $p \times m$, thus it is sure that all specimens in a high dimension can be classified. Therefore, linear kernel is applied:

$$\langle \phi(\mathbf{x}_a), \phi(\mathbf{x}_b) \rangle = \phi(\mathbf{x}_a)^T \phi(\mathbf{x}_b) = \mathbf{x}_a^T \mathbf{x}_b \quad (17)$$

The hyperplane can be solved after training SVM with massive specimens. Then detection on PCArc can be implemented by comparing a specific specimen with it.

4 Application

To verify the correctness of the proposed method, it is implemented on a HXD1C-type train: i_E is sampled and processed to detect arc with the method proposed in Sect. 3. Furthermore, a 3C device is installed on train working real-timely. Information about working state, operating events and photography on catenary could be recorded via the 3C device, which could be used as contrasts for detection.

4.1 Measurement System

The system to measure i_E which is displayed in Fig. 5, includes a sensor, a DAQ card and an upper computer. A Rog. Coil (in model of SOLAR 9301-1N) is applied to capture i_E . Cooperated with digital integrator, the effective freq. Band covers a range from DC to 200 MHz. Analog i_E is sampled via PXIe-5110 DAQ card, and transmitted to the upper computer. Sampling rate $F_s = 4$ MHz, with an 8-bit sampling depth.

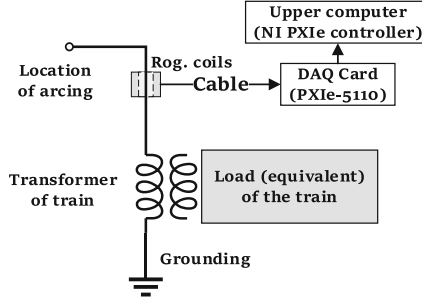


Fig. 5. Diagram to acquire signal from entry current

4.2 Construction of Datasets

On-train application contains training and validating. Data to be used in these stages is from records (label of location in km, of time and of arc) in 3C device and discrete waveform of i_E .

Training (α): Locomotive's running process from 2152.862 km to 2073.381 km is divided into 65566 fragments, with a step of 0.1s. Labels of arc are picked to serve as $y_{(\alpha,i)}$ corresponding to each fragment ($i = 1, 2, \dots, 65566$), and feature vector $\mathbf{x}_{(\alpha,i)}$ can be obtained by processing i_E in sequence. Then, the dataset of training $\mathbf{D}_\alpha = \{\mathbf{S}_{(\alpha,i)}\}$ is acquired.

Validating (β): Process from 1716.081 km to 1811.265 km is divided into 50412 fragments similarly. Labels of arc are marked as $y_{(\beta,i')}$ with $i' = 1, 2, \dots, 50412$, and feature vector $\mathbf{x}_{(\beta,i')}$ can be obtained by processing i_E . Then, the dataset of testing $\mathbf{D}_\beta = \{\mathbf{S}_{(\beta,i')}\}$ are acquired. Notion: in these specimens:

$$y_{(*)} = \begin{cases} +1, & \text{with arcing label} \\ -1, & \text{with normal label} \end{cases} \quad (18)$$

Considering generality, while solving vector $\mathbf{x}_{(*)}$, the freq. Band is divided with a multiple of 10, and the max frequency considered is 1 MHz:

$$\mathbf{F}_j = \begin{cases} [10^{j-1}, 10^j] & , j = 2, \dots, 6 \\ [0, 10^j] & , j = 1 \end{cases} \quad (19)$$

4.3 Results and Analysis

Specimens in \mathbf{D}_α are used to solve the hyperplane of SVM, then it is applied to detect PCArc according to specimens in \mathbf{D}_β . With contrasts from 3C device, accuracy of the proposed method can be estimated quantitatively.

Hyperplane of SVM

All 65566 specimens in \mathbf{D}_α are used in training: A toolbox svmtrain in MATLAB is called, with default configurations, and the hyperplane of SVM can be solved:

$$\begin{cases} \boldsymbol{\omega}^T \mathbf{x} + b = 0, & b = -0.4658 \\ \boldsymbol{\omega}^T = [0.7236, -7.1158, 10.0208, 0.6574, 0.7025, 0.0288] \end{cases} \quad (20)$$

The values of $\boldsymbol{\omega}$ in Eq. (20) illustrates: FqF2 is associated to the operation on train directly, thus it contains the 2nd largest weight. However, a lot of factors on train is linked to FqF2, thus detecting arc merely relying on it is still to be researched. FqF3, which represents the discrepancy in band from 100 Hz to 1 kHz, contains the largest weight, which accords with the expectation on HNC in Sect. 2. In addition, the existing of zero-Amp period results in large DC component in FqF1, which is the reason its weight is the 3rd largest. Weights of FqF4 and FqF5 are almost at the same degree with the one of FqF1, which indicates the power from kHC in freq. Domain.

Procedure of Detection

Two specimens, $\mathbf{S}_{(\beta,433)}\mathbf{S}_{(\beta,1)}$ are picked to display the whole process of detection. Their time/freq.-domain waveforms are shown in Fig. 6. Waveforms corresponding to time domain are at the top, freq.-domain ones are at the bottom.

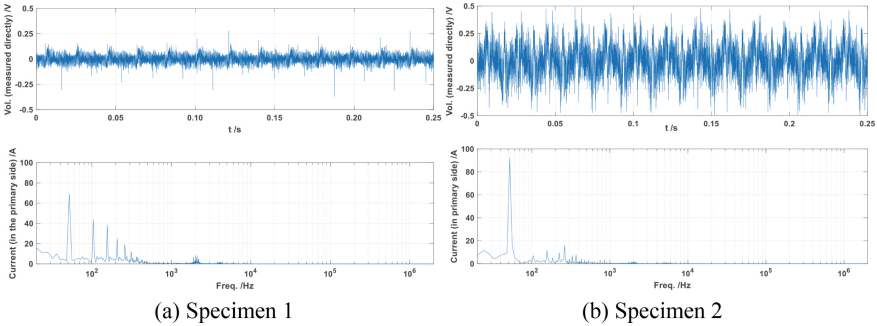


Fig. 6. Waveforms corresponding to 2 specimens in freq./time domain

In addition, values corresponding to 6 FqFs are extracted and applied in Eq. (16) in sequence, then \hat{y} could be calculated. All FqFs and \hat{y} are listed in Table 1. The values of \hat{y} accord with the arc labels from 3C device, which confirms the correctness.

Due to the large amount of testing specimens, 88 arcing and 32 normal specimens are picked to display the discrepancy on FqFs, which is shown in Fig. 7. Combined with the discussion in subsection **Hyperplane of SVM.**, values corresponding to FqF#1, #3, #4 and #5 are remarkable, which accords with the expectation as well.

Analysis on Full Results of Testing Dataset

For \mathbf{D}_β , 50412 specimens within are employed for detection: Apply their FqFs in Eq. (15), then estimates can be calculated. Comparing the results with arc labels from 3C device, a quantitative estimation on accuracy is acquired, listed in Table 2.

Table 1. Frequent features and estimate of 2 specimens

	$q''_{*,1}$	$q''_{*,2}$	$q''_{*,3}$	$q''_{*,4}$	$q''_{*,5}$	$q''_{*,6}$	\hat{y}
$S(\beta_{,433})$	2.40e-3	2.72e-3	1.88e-1	8.47e-5	3.27e-4	2.25e-4	+1.393
$S(\beta_{,1})$	3.69e-3	5.30e-4	3.03e-2	9.32e-3	8.91e-3	5.27e-4	-0.157

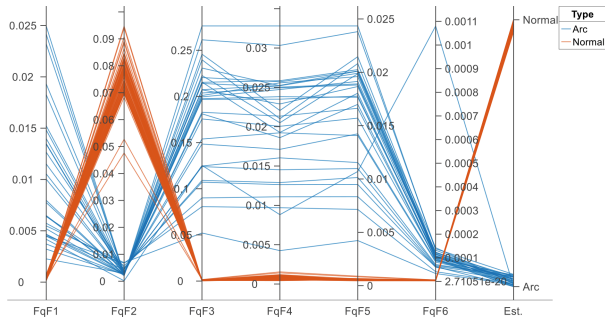


Fig. 7. Results of a portion of testing specimens

Table 2. Quantitative display for results

TP	FN	FP	TN	Miss rate (%)	FP rate (%)	Accuracy (%)
183	14	6	50209	7.11	0.012	99.96

^a In row 1, T, F, P and N denote True, False, Positive and Negative respectively
 T, opposite to F, denotes arc is detection by the proposed method
 P, opposite to N, denotes arc label is not found by 3C device

Furtherly, results of detection are checked with km-label from 3C device, then 3 sections with dense arcing-specimens are found, which are displayed in Table 3.

Table 3. Three sections with dense arcing-specimens

Section (km)	1738.930 to 1739.450	1754.547 to 1754.912	1782.589 to 1783.156
Arc-to-all	17/722	29/326	21/533

Combined with the event records from 3C device, some conclusions are inferred:
(1) In the 2nd col., 17 nearby arcing specimens are detected, while the speed of train decreasing from 53 km/h to 14 km/h sharply. An event with label “Into Station” was found in 3C device. Therefore, it’s supposed that: The arc was caused by a sudden decelerating since the train was entering into a station. **(2)** In the 3rd col., 29 nearby arcing specimens are detected, while the speed keeping steadily at a degree from 40 km/h to 45 km/h.

Moreover, no especial event was found nearby. Therefore, it's supposed: The arc might be caused due to bad quality of P-C structure. Considering this, an on-site investigation was launched, and mark of flaming was found in corresponding location of catenary. **(3)** In the last col, 21 nearby arcing specimens are detected, while the speed rising from 20 km/h to 43 km/h. An event with label "Cross insulation junction" was found, thus, it's supposed that: The arc was caused by a sudden accelerating because the train needs a high speed to get across the special location.

Above all, it is found that: The proposed method gives a reliable basic for detecting PCArc, which helps to monitor the state of P-C structure and to support on maintenance.

5 Conclusion

Aiming at the problem of arcing across P-C structure atop train, a method to detect arc based on frequency features of entry current is proposed. Conclusions includes: **(1)** Theory of generation of PCArc is studied. Frequency features especially on kHC and HNC are chosen as the base of detection. **(2)** With the discrepancy on these frequency bands, a SVM model is constructed with datasets from entry current. **(3)** This model was applied to detect PCArc on a designative railway, the accuracy is up to 99.96%. **(4)** Finally, an on-site investigation was launched, and mark of flaming was found at corresponding location of catenary, which verified the correctness.

References

1. Xie, Y., Xiao, J.: Research on high-speed railway development status and trend. *High Speed Railway Technol.* **12**(02), 23–26 (2021). (in Chinese)
2. Seo, J.H., Kim, S.W., Jung, I.H., et al.: Dynamic analysis of a pantograph catenary system using absolute nodal coordinates. *Veh. Syst. Dyn.* **44**(8), 615–630 (2006)
3. Li, B., Luo, C., Wang, Z.: Application of GWO-SVM algorithm in arc detection of pantograph. *IEEE Access*, **8**, 173865–173873 (2020)
4. Pu, W.X., Chen, T.L., Liu, B.X., Yu, L.: Study of Pantograph and catenary arc detection system based on ultraviolet light. *Instrum. Tech. Sensor* **07**, 64–67 (2014) (in Chinese)
5. Pan, G.Y.: Arc detection method for bow network based on arc sound signal characteristics. *Locomotive Rolling Stock Technol.* **328**(06), 34–36 (2017). (in Chinese)
6. Mao, Y.W., Li, H.W., Wang, R.Q.: Development of a self-powered arc-light detection system for arch networks. Automation Committee of the Chinese Railway Society. In: Proceedings of the 2017 Annual Meeting and New Technology Workshop of the Electrification Committee of the Chinese Railway Society, pp. 103–105. Electric Railway, Baoding (in Chinese)
7. Li, B., Yan, J.Y.: Research on recognition method of pantograph arc based on GAF-CNN. *J. Electron. Measure. Instrum.* **36**(1), 188–195 (2022). (in Chinese)
8. Yang, F.Q., She, P.P., Liao, Q.H., et al.: Analysis of the characteristics of pantograph-catenary arc and contact wire temperature rise during pantograph rising. *Railway Standard Des.* **66**(03), 156–161 (2022). (in Chinese)
9. Xu, W., Liu, W.Z., Yi, J.H., et al.: Study on electrical characteristics of pantograph-catenary arc during contact loss. *Railway Standard Des.* **65**(02), 147–153 (2021) (in Chinese)
10. Wang, Z.Y., Guo, F.Y., Feng, X.L., et al.: Recognition method of pantograph arc based on current signal characteristics. *Trans. China Electrotech. Soc.* **33**(01), 82–91 (2018). (in Chinese)

11. Lei, D., Zhang, T.T., Duan, X.W., et al.: Study on influence of train speed on electrical characteristics of pantograph-catenary arc **41**(7), 50–56 (2019) (in Chinese)
12. Wei, W.B., Zhang, T.T., Gao, G.Q., Wu, G.N.: Influences of pantograph-catenary arc on electrical characteristics of a traction drive system. *High Voltage Eng.* **44**(5), 1589–1597 (2018). (in Chinese)
13. Chen, X.K., Cao, B.J., Liu, Y.Y., et al.: Dynamic model of pantograph-catenary arc of train in high speed airflow field. *High Voltage Eng.* **42**(11), 3593–3600 (2016). (in Chinese)
14. Li, Z.H., Liao, X.R., Tong, Y., Chen, X.X.: Simulation and characteristic analysis of VFTO and VFTC based on a dynamic reignition arc model. *Power Syst. Protection Control* **51**(03), 79–88 (2023). (in Chinese)
15. Meng, T., Lin, X., Xu, J.Y.: Calculation of very fast transient over-voltage on the condition of segmental arcing model. *Trans. China Electrotech. Soc.* **25**(09), 69–73 (2010)